Analyst

PAPER

View Article Online
View Journal

Cite this: DOI: 10.1039/d6an00265j

DNA nanotechnology for nucleic acid analysis: detection of RNA and dsDNA amplicons using a multifunctional DNAzyme nanomachine (DNM)

Muhannad Ateiah, [a,b] Sofia S. Zablotskaya,[a] Maria S. Rubel [a,b] and Dmitry M. Kolpashchikov *[c,d]

Received 10th March 2026,
Accepted 13th April 2026

DOI: 10.1039/d6an00265j

rsc.li/analyst

DNA has long been recognized as a promising material for biotechnological applications. Here, we demonstrate how DNA nanotechnology can enhance the sensing of practically important forms of nucleic acid analytes, including folded single-stranded RNA (ssRNA) and double-stranded DNA (dsDNA) amplicons. We designed and optimized a multifunctional DNA-based sensor incorporating the catalytic 10–23 DNAzyme, herein named a DNAzyme-based nanomachine (DNM), and compared its performance with that of the classical binary 10–23 DNAzyme (BiDz) probe in detecting ssDNA, ssRNA, and dsDNA targets. The newly developed sensor exhibited up to 100- and 20-fold lower limits of detection (LODs) for ssDNA and ssRNA, respectively. Unlike traditional BiDz, DNM was capable of detecting as little as 1 μL of dsDNA amplicon, corresponding to ~2 nM PCR product in the assay, within 30 min, achieving excellent target specificity. We suggested an explanation for the behaviour of nucleic acid complexes with respect to Gibbs free energy.

Introduction

Hybridization probes are molecular tools designed to recognize specific nucleic acid sequences and report their presence, thereby enabling molecular detection and diagnostic applications. These probes exist in various formats, including molecular beacons,[1] enzyme-assisted probes[2] (*e.g.* TaqMan[3,4]), binary probes,[5] junction probes, and chemically modified probes, including locked nucleic acids (LNA), peptide nucleic acids (PNA), or invader probes.[6–8] Despite their widespread use, conventional hybridization-based probes continue to face major limitations in sensitivity and selectivity particularly when applied to folded RNA or double-stranded DNA (dsDNA) analytes.

Over time, hybridization probes have evolved from simple recognition elements into multifunctional tools capable of detecting DNA and RNA sequences with specificity towards single-nucleotide variations (SNVs), even at ambient temperatures.[5,9–11] Such precision makes them invaluable for the detection of SNVs associated with genetic disorders and cancer, as well as for the identification of bacterial resistance to antibiotics.[12–14] However, without using protein enzymes, their limits of detection (LODs) typically remain within the nanomolar range due to the absence of intrinsic signal amplification mechanisms.[15,16] The polymerase chain reaction (PCR) increases DNA analyte concentration, which can improve the overall sensitivity of PCR-based detection down to the single-molecule level.[17] However, PCR generates dsDNA amplicons that require additional processing or specialized instruments with melting or denaturation capabilities for subsequent sequence-specific detection.[18–21] Alternatively, isothermal amplification techniques such as nucleic acid sequence-based amplification (NASBA or EXPAR)[22,23] can produce ssRNA amplicons; however, these amplicons often adopt stable secondary structures that hinder their recognition by hybridization probes.[24] In this study, we detected SNVs in both dsDNA amplicons and structured ssRNA analytes using DNAzyme-based nanostructures named DNAzyme-based nanomachines (DNMs).

Binary DNAzymes (BiDz) have been applied in nucleic acid analysis since 2007 (Fig. 1A).[25] BiDz, based on the RNA-cleaving 10–23 DNAzyme,[26,27] consists of two DNA strands (Dza and Dzb) that hybridize with the target sequence to assemble a catalytic core capable of cleaving a fluorophore and quencher-labelled substrate (F-sub), thereby producing a fluorescent signal (Fig. 1A). BiDz sensors provide several advantages over conventional hybridization probes, including high specificity due to

[a]Center for Molecular and Biological Technologies, ITMO University, Lomonosova 9, St Petersburg 191002, Russia. E-mail: m.rubel@spbu.ru
[b]Laboratory of Amyloid biology, St Petersburg State University, Universitetskaya enb., 7-9, St Petersburg 199034, Russia
[c]Chemistry Department, University of Central Florida, Orlando, Florida 32816-2366, USA. E-mail: dmitry.kolpashchikov@ucf.edu
[d]Burnett School of Biomedical Sciences, University of Central Florida, Orlando, Florida 32816, USA

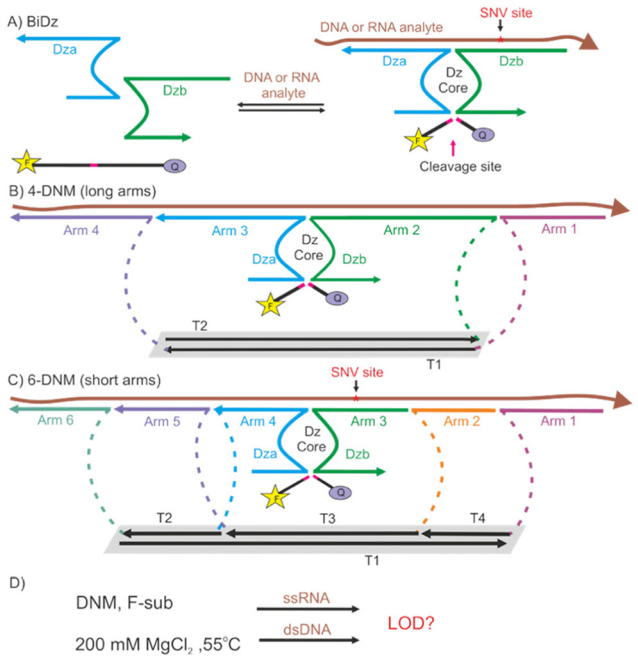

Fig. 1 Design of a 6-DNM for nucleic acid analysis. (A) Principle of the BiDz probe: two DNA strands, Dza and Dzb, bind a DNA/RNA analyte and assemble a catalytic DNAzyme (Dz) core that cleaves the fluorogenic substrate (F-sub). Dza contains longer analyte-binding arms to ensure strong analyte binding, whereas Dzb has a shorter analyte-binding arm to enhance specificity toward SNVs. (B) 4-DNM consists of arms 1, 2, and 4 attached to a dsDNA scaffold, with Arm 3 supplied from solution. (C) 6-DNM contains arms 6, 5, 4, 2, and 1 attached to the dsDNA scaffold, while the SNV-specific Arm 3 is not scaffold-bound. Strand T1 lacks an analyte-binding arm and serves as part of the dsDNA scaffold. Strands T2, T3, and T4 are linked to analyte-binding arms. Dashed lines indicate hexaethylene glycol (HEG) linkers. (D) The goal of this study is to achieve the lowest possible LOD for the best-performing DNM when detecting ssRNA and dsDNA under optimal *in vitro* sensing conditions.

their binary (split) design, low synthesis cost, and the intrinsic ability to amplify detection signals *via* Dz catalytic turnover.[28] This enables nucleic acid detection at concentrations as low as 10 pM after 3 h of incubation.[26,29,30] This represents a sensitivity over 100-fold lower than those achievable with conventional amplification-free fluorescent probes,[32,33] representing one of the most sensitive protein enzyme-free nucleic acid detection platforms reported to date. Moreover, BiDz was integrated into DNA nanostructures, further improving sensitivity using two complementary strategies: (1) F-sub delivery function[29–31] and (2) multicore catalysis.[34–36] In this study, we equipped Dz with different numbers of binding arms attached to a DNA scaffold (*e.g.* 4-DNM and 6-DNM shown in Fig. 1B and C). The multiple arms could increase target affinity and shift the hybridization equilibrium toward the formation of a stable DNM–analyte complex (Fig. 1). We aimed to achieve the lowest possible LOD for poorly accessible yet practically relevant ssRNA and dsDNA targets using DNMs. Moreover, we hypothesized that a DNM architecture composed of short analyte-binding arms (6-DNM, Fig. 1C) would minimize intramolecular self-folding, thereby enhancing target accessibility and lowering the LOD compared to long-armed DNA constructs targeting the same analyte (Fig. 1B).

Results

As a model analyte, we selected RNA-120, a unique sequence absent in the human genome and with minimal secondary structure in its single-stranded form at the assay temperature of 55 °C (Fig. S1). To generate ssRNA and dsDNA analytes, PCR amplification of the synthetic DNA template was performed using primers, one of which contained a T7 RNA polymerase promoter sequence (Fig. S2). The purified PCR product was quantified and used as the dsDNA analyte. The same PCR product served as the template for *in vitro* transcription to produce the RNA analyte (Fig. S3). The RNA product was treated with DNase, purified, and quantified as described in the SI.

Next, we designed a series of DNAzyme-based sensors with increasing numbers of analyte-binding arms. All sensors were designed to operate at 55 °C due to improved catalytic signal amplification of the DNAzyme core at elevated temperatures.[12] BiDz (Fig. S4) was designed as described earlier.[29–36] In addition, a three-armed DNM (3-DNM), a four-armed DNM (4-DNM), a five-armed DNM (5-DNM), and a six-armed DNM (6-DNM) were constructed. 6-DNM served as the full reference structure (Fig. 1C), from which the other DNM variants were derived by reducing the number of analyte-binding arms. The corresponding structures of 3-DNM, 4-DNM, 5-DNM, and 6-DNM in complex with the analyte are shown in Fig. S5A, S6A, S7A, and S8A, respectively. Specifically, 3-DNM was designed by removing arms 1, 5, and 6 from the 6-DNM structure, whereas 4-DNM was designed by merging adjacent binding arms of 6-DNM rather than by simple removal. In this design, Arm 1 remained unchanged; arms 2 and 3 were combined into a single arm, and arms 4–6 were reorganized into two longer arms, resulting in a four-arm architecture. Although the number of analyte-binding arms differs among the DNM variants, the overall length of the analyte-targeting region remains essentially the same between the 4-DNM and 6-DNM designs, with the latter segmented into a larger number of shorter arms. 5-DNM was designed by removing Arm 1 from 6-DNM.

All analyte-binding arms, except Dzb, were attached to a common DNA scaffold to ensure cooperative analyte binding, which was expected to increase the overall DNM binding affinity. This scaffold architecture differed among the DNM variants to provide the correct attachment points to each arm (Fig. S3–S6). For instance, the scaffold of 4-DNM comprised two strands (T1 and T2; Fig. 1B), the 5-DNM scaffold comprised three strands (T1, T2, and T3; Fig. S7A), and the 6-DNM scaffold comprised four strands (T1, T2, T3, and T4; Fig. 1C). Dzb was not incorporated into the assembled scaffold, thereby minimizing the chance of catalytic core formation in the absence of the target sequence and minimizing the risk of

target-independent F-sub cleavage. At the same time, the independence of the Dzb arm allows cost-effective adjustment of its affinity to the analyzed DNA or RNA without changing the sequences of the scaffold under the fixed assay temperature and buffer conditions, thus enabling selective SNV recognition.

We measured the LODs of all DNM variants across the three types of analytes— ssDNA, dsDNA, and ssRNA—and compared them with that of the classical BiDz sensor. According to our hypothesis, increasing the length of the analyte-targeting region of the DNM should enhance its ability to bind the target strand, which should be reflected by a reduced LOD.

BiDz, 4-DNM, and 6-DNM were each incubated with dsDNA and RNA analytes for 0.5 and 1 h at 55 °C. The DNMs were pre-assembled in the reaction buffer by annealing as described in the SI. Native gel analysis revealed a single band with decreased mobility, indicating the stable association of DNM-forming strands for all DNMs studied (Fig. 2, S5B, and S7B).

Table 1 lists LODs for each DNM and BiDz sensor for detecting ssDNA analytes after 0.5, 1, and 3 h of incubation with different concentrations of the DNA-120 analyte. It was found that the LOD decreased as the number of analyte-binding arms increased. The impact of the additional arms on the LOD became particularly evident during the transition from the 3-DNM to the 4-DNM design: increasing the number of analyte-binding arms from three to four, together with a simultaneous increase in the length of the sequence bound by the DNM, improved the LOD by 4.3- and 5.6-fold after 1 and 3 h of incubation, respectively. Further increases in the number of arms produced less pronounced improvements. This reduced effect reflects the structural design of the DNMs: in both 4-DNM and 6-DNM, the total length of the analyte-targeting region is essentially the same (Fig. S6A and S8A). In 6-DNM, this region is segmented into six shorter arms rather than four longer arms, resulting in comparable overall hybridization strength and similar hybridization temperatures (Tables S2 and S3). Importantly, despite targeting the same analyte region, DNMs with more binding arms exhibit a reduced LOD. We explain this result by the reduced self-folding of the short arms in 6-DNM in comparison with longer arms in 4-DNM. The resulting increase in binding affinity enabled detection at lower analyte concentrations. While further expansion of the DNM structure to target longer regions in other targets is theoretically possible, it would not only complicate assembly and the synthesis of longer oligonucleotides but also increase the likelihood of stable intra-arm secondary structures. Notably, the incorporation of additional binding arms also enables stronger signal generation at shorter incubation times, effectively reducing the required assay time. Thus, 6-DNM could detect 0.5 pM ssDNA analyte in 180 min, which is about a 94-fold improvement in comparison with the conventional BiDz sensor.

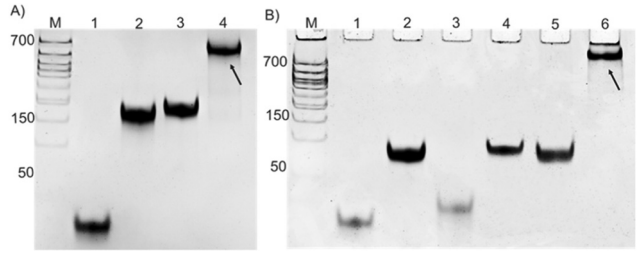

Fig. 2 Analysis of DNMs' association in 12% native polyacrylamide gel (PAGE). (A) Analysis of 4-DNM. M (Marker) – dsDNA ladder; 1 – free Arm 3; 2 – tile strand T1; 3 – tile strand T2; 4 – assembled 4-DNM (T1 and T2 strands annealed). (B) Analysis of 6-DNM association. M (Marker) – dsDNA ladder; 1 – free Dzb strand; 2 – tile strand T1; 3 – tile strand T2; 4 – tile strand T3, 5 – tile strand T4; 6 – 6-DNM (T1, T2, T3, and T4 strands annealed). The assembled DNMs are indicated by an arrow. The procedure for assembling DNMs is described in SI section 2.1. The samples were separated in 12% native PAGE at 85 V for 75 min, followed by staining with GelRed for 15 min.

Table 1 Limits of detection for the BiDz and different DNMs with the nucleic acid analytes. The graphs of the LODs for the BiDz and DNMs with the synthetic ssDNA analyte are shown in the SI (Fig. S4B, S5C, S6B, S7C, and S8B)

		LOD, pM		
		Incubation time		
Sensor	Analyte	30 min	60 min	180 min
BiDz	ssDNA	148	128	47
3-DNM		95	68	28
4-DNM		22	16	5
5-DNM		15	8	2
6-DNM		9	4	0.5
	dsDNA	173	141	90
	RNA	65	52	14

Subsequent experiments focused on 4-DNM and 6-DNM, which were selected as the most representative constructs. The performance of these sensors in detecting dsDNA and folded RNA fragments was compared with the state-of-the-art BiDz sensor.

The results show that 6-DNM produced a higher signal-to-background (S/B) ratio than 4-DNM for both dsDNA and ssRNA analytes (Fig. 3 and 4). While the binary BiDz sensor generated a detectable signal with ssRNA (Fig. 4), it failed to detect dsDNA under the same conditions. In contrast, both 4-DNM and 6-DNM successfully detected dsDNA, with 6-DNM consistently producing stronger fluorescence signals and higher S/B. These observations indicate that increasing the number of analyte-binding arms enhances signal generation

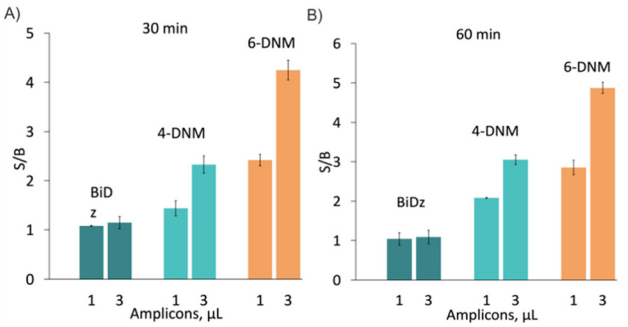

Fig. 3 Detection of dsDNA amplicons after 30 (left) and 60 (right) min of incubation at 55 °C. BiDz, 4-DNM, and 6-DNM were incubated in the presence of 1 µL (~2 nM of PCR product) or 3 µL (~6 nM of PCR product) at 55 °C for 30 min or 60 min, panels A and B, respectively. The concentration of DNA amplicons was estimated as described in the SI (Fig. S2). The data of 3 independent experiments are presented. The error bars are one standard deviation of the average.

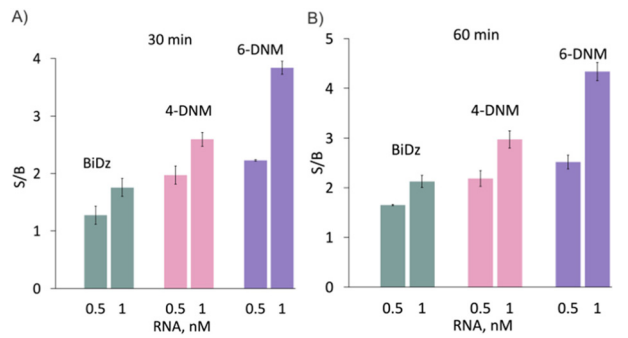

Fig. 4 Detection of RNA after 30 (left) and 60 (right) min of incubation at 55 °C. BiDz, 4-DNM, and 6-DNM were incubated in the presence of 0.5 or 1 nM of RNA at 55 °C for 30 or 60 min, panels A and B, respectively. The concentration of RNA was estimated as described in the SI. The data of 3 independent experiments are presented. The error bars are one standard deviation of the average.

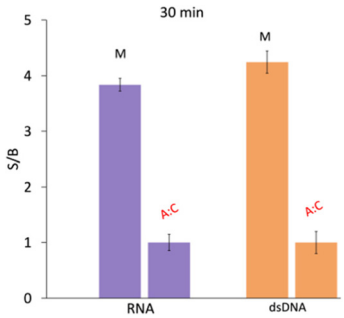

Fig. 5 6-DNM with a short SNV-sensitive Dzb arm detects RNA and dsDNA amplicons with high selectivity. Fully matched (M) and mismatched (A : C) analytes are indicated above the bars. The incubation time was 30 min at 55 °C. Selectivity factor (SF) was 99.9% for 6-DNM. SF, selectivity factor, was calculated using the formula SF = (1 − (F_{ns} − F_0)/(F_s − F_0)) × 100%, where F_0 and F_s and F_{ns} are the fluorescence intensities of the probe in the absence and in the presence of specific and non-specific analytes, respectively.

and robustness of detection for both structured RNA and dsDNA targets.

For the dsDNA target, 6-DNM achieved LODs of 141 and 90 pM after 1 and 3 h of incubation, respectively (Table 1 and Fig. S9). This LOD is sufficient for the detection of PCR products, which can be produced at concentrations ≥10 nM.[37] As expected, the ssRNA analyte was detected with lower LODs of 52 and 14 pM after 1 and 3 h, respectively. This indicates that strand invasion into dsDNA is less efficient than unwinding the RNA secondary structure, which is supported by the relative thermodynamic stability of ssRNA and dsDNA (see discussion below). Despite the higher thermodynamic stability of RNA/DNA duplexes, ssRNA targets exhibited higher LODs than ssDNA, indicating that detection sensitivity is governed primarily by target accessibility.

Importantly, increasing the number of analyte-binding arms does not compromise selectivity for both ssRNA and dsDNA targets (Fig. 5). An SNV was detected with a selectivity factor of 99.9% by the 6-DNM sensor. This high selectivity is consistent with previous studies of BiDz-based sensors.[24–29]

Discussion

In this study, we questioned whether ssRNA and dsDNA can be detected by DNMs and if sensitivity arises not only from extending the analyte-binding region, but also from segmentation of the analyte-binding arms into shorter segments. The multivalent organization could reduce self-folding and increase binding affinity and sensitivity. The enhanced performance of DNM relative to conventional BiDz sensors arises from the increased thermodynamic stability of the analyte–sensor complex enabled by their multivalent, pre-organized architecture. In the DNM design, multiple analyte-binding arms are interconnected within a rigid scaffold. Such a pre-organization minimizes the entropic penalty of multivalent hybridization and enhances the thermodynamic stability of the analyte–sensor complex, thereby increasing the effective local concentration of the catalytically active 10–23 DNAzyme core.[38] The role of linker flexibility has been previously investigated in related systems, where increased flexibility resulted in an improved S/B ratio without significantly affecting the LOD or selectivity.[39] These findings support the role of flexible linkers in facilitating cooperative binding while preserving the effective spatial organization of the sensing complex. At the same time, the role of linkers in the context of each DNM system warrants further systematic investigation. In addition, the scaffolded architecture stabilizes the sensing complex by enabling rapid rebinding of transiently dissociated arms, reducing the probability of complete complex dissociation and promoting sustained catalytic activity.

For the ssDNA analyte, the advantages of the DNM architecture translate directly into improved sensitivity relative to the BiDz sensor. Because ssDNA lacks stable secondary structure, detection in this system primarily reflects intrinsic differences

in sensor design rather than target accessibility. Thermodynamic analysis reveals a progressive stabilization of the analyte–sensor complex with an increasing number of binding arms, with a calculated ΔG of −60.16 kcal mol^{-1} for the BiDz–ssDNA complex, −95.1 kcal mol^{-1} for the 4-DNM–ssDNA complex, and −105.1 kcal mol^{-1} for the 6-DNM–ssDNA complex (Table S3). This monotonic trend correlates with the observed improvement in the LOD for ssDNA targets, indicating that cumulative hybridization strength plays a dominant role under these conditions. Notably, the additional stabilization observed for 6-DNM relative to 4-DNM does not arise from an increase in the total length of the analyte-binding region, which is essentially identical in both designs, but rather from differences in the intrinsic folding thermodynamics of the sensor itself. Segmentation of the analyte-binding region into a larger number of shorter arms in 6-DNM, combined with their incorporation into a more extended scaffold, reduces the stability of sensor self-folding (ΔG_fold ≈ −6.7 kcal mol^{-1} for 6-DNM *versus* −11.9 kcal mol^{-1} for 4-DNM). This decrease in intramolecular stabilization lowers the energetic penalty for sensor opening upon target binding, thereby contributing to a more favourable ΔG for the formation of the 6-DNM–ssDNA complex. Importantly, the observed LOD for ssDNA (0.5 pM) is approximately 1000-fold lower than that reported for typical hybridization probes, including molecular beacons[32] and light-up aptamer sensors.[33]

Detection of structured ssRNA introduces additional constraints associated with intramolecular folding, which limit continuous access to complementary sequences despite the single-stranded nature of the target. While both ssDNA and ssRNA can adopt secondary structures, RNA folding is generally more stable and persistent, introducing a larger energetic penalty for target opening and rendering effective sensor binding less favourable than for ssDNA. Thermodynamic analysis nevertheless reveals that the formation of the DNM–ssRNA complex is highly favourable, with calculated ΔG values of −49.1 kcal mol^{-1} for BiDz–ssRNA, −88.9 kcal mol^{-1} for 4-DNM–ssRNA, and −96.0 kcal mol^{-1} for 6-DNM–ssRNA (Table S3). Consequently, the accessibility of RNA target regions is transient rather than continuous. Consistent with this behaviour, hybridization to RNA targets can be initiated at exposed structural elements such as hairpin loops.[40,41] In this context, multivalent DNMs provide a distinct advantage by enabling sequential engagement of such transiently accessible RNA segments. Once partial hybridization is established, additional binding arms can interact with nearby regions before refolding occurs, stabilizing the opened conformation and promoting formation of the catalytically active complex. This cooperative capture of transiently accessible states enables efficient recognition of structured RNA despite intramolecular folding. Nevertheless, the increased stability of the RNA secondary structure reduces the thermodynamic stability of the 6-DNM–ssRNA complex relative to the 6-DNM–ssDNA complex, resulting in higher LOD. Thus, ssRNA targets are detected with 7- to 40-fold lower sensitivity (depending on incubation time) than ssDNA, reflecting the difference in the stability of analyte secondary structures rather than the stability of the DNM–analyte complex. Still, detection down to 14 pM was achieved, which is among the lowest LODs reported for structured RNA. Importantly, traditional hybridization sensors, such as molecular beacon probes, often fail to detect folded ssDNA or ssRNA analytes.[41,42]

Thermodynamic analysis predicts a strongly unfavourable ΔG for dsDNA recognition by the BiDz sensor (ΔG ≈ +57.4 kcal mol^{-1}), which explains its inability to generate a detectable fluorescent signal with dsDNA targets. In contrast, increasing the number of analyte-binding arms substantially reduces the overall energetic cost associated with strand invasion, yielding ΔG values of +17.6 and +12.5 kcal mol^{-1} for 4-DNM and 6-DNM, respectively (Table S3). This marked reduction correlates with the experimental observation that both DNMs successfully detect dsDNA, whereas BiDz does not.

Strand invasion by DNMs is likely initiated through transient local opening ("breathing") of the dsDNA duplex, which provides short-lived access to complementary sequences. Binding of an initial arm stabilizes these transiently accessible regions and facilitates subsequent engagement of neighbouring arms due to their high effective local concentration within the scaffold. This cooperative, multivalent mechanism enables stabilization of partially invaded states without requiring complete strand displacement.

Detection in this system does not require binding of a large fraction of the dsDNA target. Given a limit of detection in the picomolar range and typical dsDNA amplicon concentrations reaching tens of nanomolar, the formation of only a small fraction ($\lesssim$1%) of 6-DNM–dsDNA complexes is sufficient to generate a detectable signal due to the catalytic turnover. 6-DNM achieved S/B in the presence of ∼2 nM dsDNA in 60 min (Fig. 3B); the same S/B ratio was achieved by 6-DNM in the presence of 40 pM ssDNA analyte. Assuming that after 3 h of incubation, the system reached equilibrium and that 6-DNM binds nearly all of the 40 pM ssDNA analyte, we can estimate that only about 1.3% of dsDNA amplicons form a complex with 6-DNM under the reaction conditions. However, the comprehensive thermodynamic studies on DNM invasion into a dsDNA target should be performed separately.

Importantly, increasing the number of analyte-binding arms does not compromise sequence selectivity. Single-nucleotide discrimination is preserved through the binary DNAzyme design, which requires correct hybridization of both Dza and Dzb arms for catalytic core formation, with one arm remaining unincorporated into the preassembled scaffold. A logical next step is to investigate strategies for determining the optimal number of segments within the DNA nanomachine architecture. In particular, it will be important to assess whether very short fragments (5–10 nt), when attached to a scaffold, can further enhance the design and performance of DNM-based sensors.

Collectively, these results establish multivalent DNMs as versatile and sensitive platforms for nucleic acid detection across structurally distinct target classes, including ssDNA,

structured ssRNA, and dsDNA amplicons. By enabling detection at picomolar concentrations without target denaturation, DNMs are well suited for analysis of PCR products, structured RNA transcripts, and clinically relevant SNVs. The modular architecture of DNMs provides a general design framework for tuning sensitivity, assay time, and target compatibility, highlighting their potential for diagnostic applications where rapid, selective, and amplification-free detection is required. Recent advances in amplification-free nucleic acid sensing further underscore the potential of highly sensitive probe-based detection systems.[43,44] It is important to note that the DNM design holds significant potential for improving sensor–analyte hybridization kinetics, which will be addressed in a separate study.

Conclusions

By systematically increasing the number of analyte-binding arms, we demonstrate that cooperative DNM architectures substantially enhance target detection and reduce LODs for ssRNA and dsDNA analytes. 6-DNM, equipped with 6 short analyte-binding arms, exhibited the best overall performance, achieving the lowest LODs in shorter times without compromising SNV discrimination. These findings indicate that, in addition to expanding the analyte-binding region, partitioning long arms into shorter segments can further improve the sensitivity of multicomponent hybridization probes. This versatility highlights the potential of DNMs for detecting structured RNAs and PCR-generated dsDNA amplicons under isothermal conditions, without requiring denaturation or additional processing. Overall, the cooperative multi-arm DNM architecture represents a significant advancement in enzyme-free nucleic acid detection. Its combination of high sensitivity, rapid response, modularity, and robust SNV discrimination positions it as a powerful and adaptable tool for diagnostic applications ranging from pathogen detection to genotyping and point-of-care testing.

Author contributions

M. A. obtained, collected, and analysed the data and wrote the manuscript. S. S. Z. collected the experimental data. M. S. R. and D. M. K. conceived the idea and participated in the research design and data analysis. All authors participated in writing and editing the manuscript.

Conflicts of interest

The authors declare no conflicts of interest.

Data availability

All data supporting the findings of this study are included in the article and the supplementary information (SI). Supplementary information: figures, materials and methods. See DOI: https://doi.org/10.1039/d6an00265j.

Acknowledgements

The authors thank Ilya Veligzhaninov for the RNA/DNA-120 sequence development. The project was funded by RSCF and SPbSCF (project 25-16-20127). Muhannad Ateiah acknowledges project no. FSER-2025-0019 for chemical modelling.

References

1 S. Tyagi and F. R. Kramer, *Nat. Biotechnol.*, 1996, **14**, 303–308.
2 Y. V. Gerasimova and D. M. Kolpashchikov, *Chem. Soc. Rev.*, 2014, **43**, 6405–6438.
3 Y. Kim, D. Sohn and W. Tan, *Int. J. Clin. Exp. Pathol.*, 2008, **1**, 105–116.
4 F. Pellestor and P. Paulasova, *Eur. J. Hum. Genet.*, 2004, **12**, 694–700.
5 D. M. Kolpashchikov, *Chem. Rev.*, 2010, **110**, 4709–4723.
6 D. K. Darnell and P. B. Antin, *Methods Mol. Biol.*, 2014, **1211**, 69–76.
7 P. Zhang, T. Beck and W. Tan, *Angew. Chem., Int. Ed.*, 2001, **40**, 402–405.
8 P. J. Hrdlicka and M. E. Everly, *RSC Chem. Biol.*, 2026, **7**, 323–351.
9 D. M. Kolpashchikov, *Acc. Chem. Res.*, 2019, **52**, 1949–1956.
10 A. Sarwar, F. Shakeel, T. Fatima, R. Amin, S. N. B. Rizvi, T. Hussain and A. Afzal, *Int. J. Biol. Macromol.*, 2025, **329**, 147825.
11 D. Huang, Y. Liu, G. A. Wang, S. Lv, Y. Tan and F. Li, *Chem. Soc. Rev.*, 2026, **55**, 714–764.
12 S. M. Bone, N. J. Hasick, N. E. Lima, S. M. Erskine, E. Mokany and A. V. Todd, *Anal. Chem.*, 2014, **86**, 9106–9113.
13 Y. He, K. Zeng, A. S. Gurung, M. Baloda, H. Xu, X. Zhang and G. Liu, *Anal. Chem.*, 2010, **82**, 7169–7177.
14 H. N. Bengtson, S. Homolka, S. Niemann, A. J. Reis, P. E. da Silva, Y. V. Gerasimova, D. M. Kolpashchikov and K. H. Rohde, *Biosens. Bioelectron.*, 2017, **94**, 176–181.
15 C. Xi, M. Balberg, S. A. Boppart and L. Raskin, *Appl. Environ. Microbiol.*, 2003, **69**, 5673–5678.
16 J. J. Li, Y. Chu, B. Y. Lee and X. S. Xie, *Nucleic Acids Res.*, 2008, **36**, e36.
17 M. Owusu, B. Nkrumah, G. Acheampong, S. Opoku Afriyie, E. K. Addae, R. Larbi, R. O. Ansah, C. Kubio, F. Saeed, N. K. Ayisi-Boateng, E. Darko, J. Amonoo-Neizer, A. G. Owusu-Ansah, F. Ayensu, P. K. Brenya, V. Bannor,

P. Angra and D. T. Barradas, *Microbiol. Spectrum*, 2025, **13**, e03219–e03224.
18 K. E. Pierce and L. J. Wangh, *Methods Mol. Biol.*, 2011, **688**, 47–66.
19 A. Brinker, H. Schulze, T. Bachmann and R. Möller, *Biosens. Bioelectron.*, 2010, **26**, 898–902.
20 B. Faltin, R. Zengerle and F. von Stetten, *Clin. Chem.*, 2013, **59**, 1567–1582.
21 J. Guo, J. Ju and N. J. Turro, *Anal. Bioanal. Chem.*, 2012, **402**, 3115–3125.
22 Q. Wu, C. Suo, T. Brown, T. Wang, S. A. Teichmann and A. R. Bassett, *Sci. Adv.*, 2021, **7**, eabe5054.
23 X. Ou, K. Li, M. Liu, J. Song, Z. Zuo and Y. Guo, *Analyst*, 2024, **149**, 4135–4157.
24 D. A. Gorbenko, L. A. Shkodenko, M. S. Rubel, A. V. Slita, E. V. Nikitina, E. A. Martens and D. M. Kolpashchikov, *Chem. Commun.*, 2022, **58**, 5395–5398.
25 D. M. Kolpashchikov, *ChemBioChem*, 2007, **8**, 2039–2042.
26 E. Mokany, S. M. Bone, P. E. Young, T. B. Doan and A. V. Todd, *J. Am. Chem. Soc.*, 2010, **132**, 1051–1059.
27 S. M. Bone, N. J. Hasick, N. E. Lima, S. M. Erskine, E. Mokany and A. V. Todd, *Anal. Chem.*, 2014, **86**, 9106–9113.
28 S. W. Santoro and G. F. Joyce, *Proc. Natl. Acad. Sci. U. S. A.*, 1997, **94**, 4262–4266.
29 A. J. Cox, H. N. Bengtson, K. H. Rohde and D. M. Kolpashchikov, *Chem. Commun.*, 2016, **52**, 14318–14321.
30 Z. Hussein, M. A. Y. Nour, A. V. Kozlova, D. M. Kolpashchikov, A. B. Komissarov and A. A. Eldeeb, *Anal. Chem.*, 2023, **95**, 18667–18672.
31 V. V. Solyanikova, D. A. Gorbenko, V. V. Zryacheva, A. A. Shtro and M. S. Rubel, *Int. J. Mol. Sci.*, 2025, **26**, 3652.
32 D. M. Kolpashchikov, *Scientifica*, 2012, **2012**, 928783.
33 D. M. Kolpashchikov and A. A. Spelkov, *Angew. Chem., Int. Ed.*, 2021, **60**, 4988–4999.
34 Z. Hussein, L. A. Golovina, M. Alaji, M. A. Y. Nour, D. M. Kolpashchikov, A. B. Komissarov and A. A. Eldeeb, *ChemBioChem*, 2024, **25**, e202400572.
35 T. A. Lyalina, E. A. Goncharova, N. Y. Prokofeva, E. S. Voroshilina and D. M. Kolpashchikov, *Analyst*, 2019, **144**, 416–420.
36 A. A. Eldeeb, S. S. Zablotskaya, M. S. Rubel, M. A. Y. Nour, L. I. Kozlovskaya, A. A. Shtro, A. B. Komissarov and D. M. Kolpashchikov, *ChemMedChem*, 2022, **17**, e202200382.
37 R. K. Saiki, D. H. Gelfand, S. Stoffel, S. J. Scharf, R. Higuchi, G. T. Horn, K. B. Mullis and H. A. Erlich, *Science*, 1988, **239**, 487–491.
38 D. D. Nedorezova, M. V. Dubovichenko, A. A. El-Deeb, M. A. Y. Nour, G. A. Bobkov, A. I. Ashmarova, A. J. Kalnin and D. M. Kolpashchikov, *Chem. – Eur. J.*, 2024, **30**, e202401580.
39 B. L. Mueller, M. J. Liberman and D. M. Kolpashchikov, *Nanoscale*, 2023, **15**, 5735–5742.
40 M. Ateiah, E. R. Gandalipov, A. A. Rubel, M. S. Rubel and D. M. Kolpashchikov, *Int. J. Mol. Sci.*, 2023, **24**, 4473.
41 Y. V. Gerasimova and D. M. Kolpashchikov, *Biosens. Bioelectron.*, 2013, **41**, 386–390.
42 C. Nguyen, J. Grimes, Y. V. Gerasimova and D. M. Kolpashchikov, *Chemistry*, 2011, **17**, 13052–13058.
43 H. Hendra, W. Leesutthiphonchai, N. Kuncharoen, S. Kasem, O. Chailapakul, T. Ozer, S. Jampasa and T. Chatnaparat, *Mikrochim. Acta*, 2025, **192**, 541.
44 A. Lomae, K. Teekayupak, P. Preechakasedkit, E. Pasomsub, T. Ozer, C. S. Henry, D. Citterio, T. Vilaivan, O. Chailapakul and N. Ruecha, *Talanta*, 2024, **279**, 126613.